The University of Bern Atmospheric Ion Model: Time-dependent modeling of the ions in the mesosphere and lower thermosphere

Jan Kazil and Ernest Kopp
Space Research and Planetary Sciences, University of Bern, Bern, Switzerland

Simon Chabrillat
Belgian Institute for Space Aeronomy, Brussels, Belgium

James Bishop
Naval Research Laboratory, Washington, D. C., USA

Received 8 October 2002; revised 4 April 2003; accepted 24 April 2003; published 31 July 2003.

[1] In this paper the first time-dependent model of ion chemistry in the mesosphere/lower thermosphere (MLT) region acting within a global, time-dependent, two-dimensional neutral atmosphere model is described. Selected diurnal results are presented for undisturbed solar minimum conditions. The University of Bern Atmospheric Ion Model (UBAIM) is a time-dependent, pseudo-two-dimensional model of the ion chemistry in the Earth atmosphere. It covers latitudes from 85°S to 85°N and (log-pressure) altitudes from 20 to 120 km. On this grid a system of differential equations describing the ion chemistry is integrated numerically until a periodical solution, governed by the diurnal changes in the incident radiation, is reached; this solution constitutes a model for quiet or undisturbed conditions. The basic ion chemistry of the UBAIM contains 311 reactions for 71 charged species. Ionization sources are solar X-ray and EUV radiation, resonantly scattered Lyman α and β photons, and galactic cosmic rays. Densities of main and trace neutral atmospheric constituents are taken from a new version of the bidimensional NCAR model SOCRATES, which has been specifically optimized for mesospheric and lower thermospheric processes with upper boundary conditions set using the empirical MSIS thermosphere model. Direct solar flux inputs are computed by the SOLAR2000 model; scattered Lyman α and β fluxes are calculated using geocoronal hydrogen density profiles consistent with the adopted MSIS density distributions. *INDEX TERMS:* 0310 Atmospheric Composition and Structure: Airglow and aurora; 0335 Atmospheric Composition and Structure: Ion chemistry of the atmosphere (2419, 2427); 0340 Atmospheric Composition and Structure: Middle atmosphere—composition and chemistry; 2427 Ionosphere: Ionosphere/atmosphere interactions (0335); 2419 Ionosphere: Ion chemistry and composition (0335); *KEYWORDS:* ion chemistry, D-region, lower E-region, ion model, ionization

Citation: Kazil, J., E. Kopp, S. Chabrillat, and J. Bishop, The University of Bern Atmospheric Ion Model: Time-dependent modeling of the ions in the mesosphere and lower thermosphere, *J. Geophys. Res.*, *108*(D14), 4432, doi:10.1029/2002JD003024, 2003.

1. Introduction

1.1. Ions in the Stratosphere, Mesosphere, and Lower Thermosphere

[2] Our knowledge of the ion composition in the Earth's atmosphere is based mostly on in situ mass spectrometric measurements and on laboratory investigations of the various processes of ion chemistry. In the high-density part of the middle atmosphere (below about 80 km) it has been necessary to use cryogenically pumped instruments on sounding rockets and balloon payloads. In order to avoid the break-up of loosely bound cluster ions, these instruments operate with low ion attracting electric fields and with conically shaped inlet geometries on the rocket-borne instruments to reduce or prevent the formation of shock fronts.

[3] The formation and chemistry of positive ions in the lower thermosphere, mesosphere, and stratosphere are relatively well understood, and the positive ion composition has been explored in various campaigns [e.g., *Smith*, 1970; *Zbinden et al.*, 1975; *Herrmann et al.*, 1978; *Kopp et al.*, 1978; *Arijs et al.*, 1982a; *Kopp et al.*, 1985]. The initial ions NO^+ and O_2^+ dominating the lower thermosphere are rapidly lost below 80 km in a well-known set of clustering reactions, ending up in a stable family of pure proton hydrates $H^+(H_2O)_n$ with a hydration order n between 2 and 7, depending on the water vapor density

0148-0227/03/2002JD003024

and the ambient temperature. In the stratosphere the abundance of pure proton hydrates is reduced through switching reactions of water ligands with acetonitrile (CH_3CN) and with other molecules having a higher proton affinity than water. The major positive ions in the stratosphere are thus mixed proton hydrates [*Arijs et al.*, 1980; *Smith et al.*, 1981].

[4] Negative ions occur below approximately 80 km, where the total atmospheric density is sufficiently high to enable the attachment of electrons to oxygen in three-body reactions. In the subsequent ion chemistry, well-known molecular ions (for example, CO_3^-, NO_3^-, and Cl^-) are formed. At lower altitudes these molecular ions serve as cores of cluster ions, which are formed in the presence of molecules having a high electron affinity, such as H_2SO_4. These molecules play a major role in the negative ion chemistry even if occurring at ppt levels. A series of such trace gases exists in the stratosphere affecting the negative ion population.

[5] In situ balloon and rocket measurements of negative ions in the past were much less frequent and suffered in several flights from reduced instrument sensitivity due to negative charging effects on the rocket payload or the balloon surface. The few good measurements of the negative ions showed large variability and mass spectra distributed over a broad range up to 200 amu, including cluster ions of the form $X^-(HNO_3)_n$, $X^-(H_2SO_4)_n$, and $X^-(HCl)_n$ [*Arnold et al.*, 1971; *McCrumb and Arnold*, 1981; *Arnold et al.*, 1981; *Arijs et al.*, 1982b, 1983].

[6] Some of the low-mass negative ions also have a loosely bound electron, which can be detached by sunlight even in the visible range. Owing to this effect the photochemistry of negative ions and the occurrence of free electrons show strong diurnal variations. A related phenomenon is the variability of the lower boundary of the ionosphere, typically ranging from about 60 km at noon to 90 km at midnight.

[7] Below approximately 65 km, ion production is mainly from galactic cosmic ray precipitation and is therefore much more steady in the stratosphere and lower mesosphere than at higher altitudes. Only occasionally, during intense solar flare events or at high latitudes through energetic auroral precipitation, ion production can be locally enhanced by several orders of magnitude; such events are, however, rather rare and limited in time with durations of hours to a few days.

[8] In order to extend knowledge on the ion composition of the atmosphere beyond the findings of in situ measurements, which inevitably cover only isolated segments of space and time, a number of numerical models have been developed in past decades, as will be discussed next. However, owing to lack of data on ion chemistry and on abundances of atmospheric tracers, the forecasting abilities of these models have remained limited.

1.2. Earlier Modeling Efforts

[9] The first time-dependent model of the lower ionosphere was presented in 1970 by *Keneshea et al.* [1970], who computed NO^+, O_2^+ and electron concentrations between 85 and 140 km as a function of solar zenith angle. One year later, *Arnold and Krankowsky* [1971] compared their model calculations with rocket flight mass spectrometer nighttime data with an emphasis on negative ions (in particular on CO_3^- and NO_3^-) between 65 and 85 km. *Jones and Rees* [1973] investigated ion composition in a time varying aurora, including the buildup and decay of ions and electrons during auroral precipitation events. *Turco and Sechrist* [1972a, 1972b, 1972c] used a time-dependent model in a series of studies focusing on the sunrise D-region. They investigated the importance of photodetachment, morning formation of ozone, atomic and metastable oxygen $O_2(^1\Delta_g)$ for the formation of the early morning electron layer. *Thomas et al.* [1973] showed in their model of the D-region that photodetachment is an important process in accounting for the observed daytime electron densities below 70 km. *Strobel et al.* [1974] conducted a detailed numerical study of the nighttime ionosphere to quantify the importance of the different ionization sources at night. They presented model results for nighttime fluxes of the hydrogen lines at 121.6 nm and 102.6 nm and of the helium lines at 58.4 nm and 30.4 nm (He^+), finding that nighttime Lyman α and β are sufficient to account for observed electron densities in the lower thermosphere. In a subsequent study [*Strobel et al.*, 1980] the importance of starlight on nighttime ionization in the E- and F-regions was investigated. *Thomas* [1976a] constructed a model of daytime positive ion D-region chemistry, investigating in particular the clustering reactions of NO^+ with CO_2 and N_2 with respect to the hydration of NO^+. *Wisemberg and Kockarts* [1980] presented an ion model of the mesosphere with a complex negative chemistry and evaluated quantitatively the importance of the various paths in the model.

[10] *Fehsenfeld and Albritton* [1980] suggested a stratospheric and tropospheric ion chemistry that included HNO_3 and H_2SO_4 in the negative part. In 1983, *Brasseur and Chatel* [1983] presented an initial ion model of the stratosphere, including a complex ion chemistry of H_2SO_4, which was followed by *Kawamoto and Ogawa* [1984]. *Thomas and Bowman* [1985] created a time-dependent D-region model, which computed periodic solutions of the system of differential equations describing the ion chemistry, similar to the approach taken in this paper but without investigating ion density diurnal cycles. In a subsequent study they investigated the increase in lower D-region electron density before sea level sunrise [*Thomas and Bowman*, 1986]. *Brasseur and De Baets* [1986] presented the model carrying their name, where they combined for the first time a steady state ion model with a two-dimensional neutral model and used it to study the seasonal and latitudinal variability of the ion composition and its dependence on trace gas variability and temperature. Later, *Arijs and Brasseur* [1986] combined a one-dimensional neutral model of CH_3CN with a complex ion chemistry of this species to compute the mixed proton clusters $H^+(H_2O)_n(CH_3CN)_m$. A conceptually different model has been developed at the Sodankylä Geophysical Observatory [*Burns et al.*, 1991; *Turunen*, 1993; *Turunen et al.*, 1993], containing a detailed chemical scheme to be used as a tool in the interpretation of D-region incoherent scatter experiments and cosmic radio noise absorption measurements. *Beig et al.* [1993a, 1993b] presented a two-dimensional model of the ion composition in the stratosphere, which not only accounted for mixed proton hydrates (containing

CH_3CN) but also for negative cluster ions with NO_3^- and HSO_4^- cores.

1.3. History of the UBAIM

[11] The first version of UBAIM was published by *Kull et al.* [1995] and covered the low and middle latitude mesosphere. Its chemistry was based on the work of *Reid* [1976, 1977] and *Thomas* [1976a, 1976b] in the positive part and on the work of *Wisemberg and Kockarts* [1980], *Thomas* [1983], and *Thomas and Bowman* [1985] in the negative part. An improved version extended with reactions from the *Brasseur and De Baets* [1986] model has been published 1997 by *Kull et al.* [1997]. The ionization sources were galactic cosmic rays [*Heaps*, 1978] and Lyman α.

[12] In 1997, *Fritzenwallner and Kopp* [1997a] extended the model into the high latitudes and into the lower thermosphere, and included solar EUV [*Hinteregger et al.*, 1981; *Torr and Torr*, 1985; *Richards et al.*, 1994] and X-rays as ionization sources. In a subsequent study, *Fritzenwallner and Kopp* [1997b] modeled the ionic and neutral chemistry of the major thermospheric metals Na, Si, Fe, and Mg by solving the diffusion (eddy- and molecular) equation numerically. Chlorine and bromine ions were introduced and discussed by *Fritzenwallner and Kopp* [1997c], as well as the formation of negative cluster ions in the mesosphere [*Fritzenwallner and Kopp*, 1998]. These model versions provided the ion densities in steady state for a certain time of day.

[13] The model presented in this publication differs greatly from these previous versions and represents the first attempt to use a time-dependent neutral background atmosphere provided by a global two-dimensional (2-D) model in a time-dependent ion model of the MLT region.

2. Model Description

[14] A short description of the University of Bern Atmospheric Ion Model (Version 5.25) and of its inputs is given here. Readers interested in the details of the implementation are referred to *Kazil* [2002]. The UBAIM input is taken from the neutral atmosphere models SOCRATES [*Chabrillat*, 2001] and MSISE [*Hedin*, 1991], the solar flux model SOLAR2000 [*Tobiska et al.*, 2000], and from a sophisticated model of scattered solar Lyman α and β flux [*Bishop*, 2001, 1991].

[15] The UBAIM is a time-dependent, decoupled pseudo-two-dimensional model, acting within a background atmosphere produced by a two-dimensional global model of atmospheric dynamics and composition. The term ''pseudo-two-dimensional'' refers to the fact that the UBAIM divides the 2-D background atmosphere into a set of boxes which do not exchange particles with each other. This is valid for ions with short lifetimes (at the order of minutes). The UBAIM is decoupled, since the ion composition is modeled without feedback to the background atmosphere. This is legitimate as in the undisturbed lower ionosphere, the maximum charged pairs volume mixing ratio is typically less than 150 ppb.

2.1. Background Atmosphere: SOCRATES Update

[16] The temperature and densities of the neutral species are computed by a new version of the two-dimensional model SOCRATES, which calculates interactively the wind field, the chemical composition and the temperature between 85° south and 85° north, and from the surface to 120 km log-pressure altitude. We give here a brief summary of the modifications brought to the model since it was described by *Brasseur et al.* [2000] and *Khosravi et al.* [2002]. For a full description the reader is referred to *Chabrillat* [2001].

[17] Molecular diffusion is taken into account for all species and at all altitudes in the middle atmosphere using a new mass-conservative algorithm. While this process is important for carbon dioxide and temperature at mesopause levels [*Chabrillat et al.*, 2002], it also plays a role in the distribution of species lighter than air, such as water vapor: molecular diffusion imposes an upward flux on these species. The default upper boundary condition (null flux) can not be used for these species, and volume mixing ratios (vmr) are prescribed instead.

[18] The upper boundary conditions on temperature and on the volume mixing ratios (vmr) of H, $O(^3P)$ and O_2 come from the semiempirical model MSISE-90 [*Hedin*, 1991]. The vmr of H_2, H_2O, and CH_4 are set to 3.5 ppm, 0.1 ppm, and 1 ppb, respectively, at the upper boundary. All other chemical species have a null flux as upper boundary condition, except for NO.

[19] In the lower thermosphere, nitrogen monoxide (nitric oxide) is subject to considerable temporal and spatial variability and can reach very high concentrations. We implemented in SOCRATES crude parameterizations to represent the chemical effects of the processes responsible for thermospheric NO production. At the upper boundary we set a downward flux of NO molecules of photoelectron-impact origin [*Solomon et al.*, 1982]. A special photoelectron-impact production is also imposed above 100 km altitude [*Siskind and Rusch*, 1992], as well as auroral-related production in the polar regions [*Mc Ewan and Phillips*, 1975]. These parameterizations have been reduced by a factor of two to reach the climatological abundances observed at solar minimum activity [*Siskind et al.*, 1998].

[20] Residual circulation in the mesosphere is characterized by a rising motion in the summer hemisphere and a sinking motion in the winter hemisphere, responsible for the latitudinal gradients of temperature observed in the mesosphere. This residual circulation is due to momentum deposition by gravity wave breaking, a dynamical forcing which was previously evaluated by the classical parameterization of *Lindzen* [1981].

[21] Momentum deposition by gravity wave breaking is now prescribed by a function of altitude, latitude, and season and has been carefully adjusted so that the modelled mesospheric temperatures closely match the MSISE-90 climatological distributions throughout the year. The feedback between the zonal wind field and the temperature is lost, but our two-dimensional model is now able to reproduce quite precisely the the two-level structure of the mesopause and the very low temperatures reached during summer [*She and von Zahn*, 1998; *Berger and von Zahn*, 1999].

[22] Several enhancements have been implemented to fulfill the specific requirements of the UBAIM model. Since O_2^+ is produced by photoionization of $O_2(^1\Delta_g)$, we added $O_2(^1\Sigma)$ and $O_2(^1\Delta_g)$ in the species list, using the photochemical scheme presented by *Mlynczak et al.* [1993]; this includes the direct excitation of molecular oxygen from the

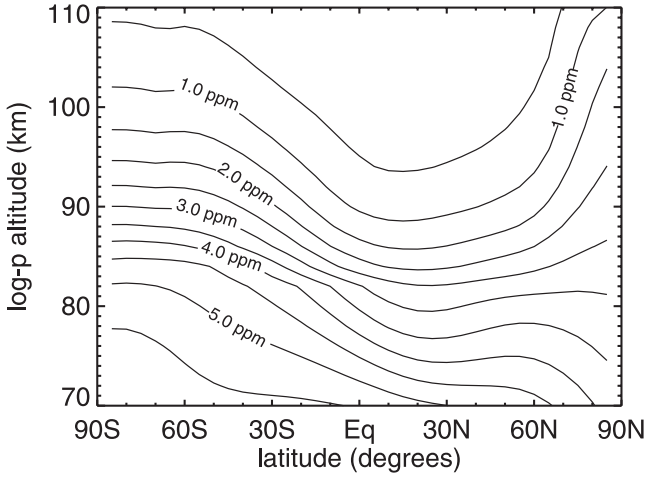

Figure 1. Volume mixing ratio of water vapor, 1996-12-21, 1200, computed by SOCRATES. Contour step is 0.5 ppm.

ground state to $O_2(^1\Sigma)$ by absorption of solar radiation at 762 nm, using the photoexcitation rate parameterization of *Mlynczak* [1993].

[23] In all previous versions of SOCRATES the chemistry was solved using latitude-dependent timesteps, and the transport was solved once per day. As a result, the diurnal cycles of many species displayed large discontinuities. The timestep for the chemistry is now constant, and the advection by the residual winds is applied after each resolution of the chemical system. This timestep is set to 5 min to generate the high-resolution output required by UBAIM. The calculation of the photolysis and solar heating rates takes into account the altitude dependency of the local time at sunrise and sunset.

[24] Finally, to circumvent the problem of water vapor transport across the tropopause, the lower boundary for H_2O was raised from the surface to 17 km *log-p* altitude. The boundary condition at this level is the monthly climatological average of the UARS/HALOE measurements [*Randel et al.*, 1998]. This allows SOCRATES to compute a realistic distribution and annual variation of H_2O in the stratosphere and the mesosphere.

[25] All calculations for the present study were performed at solar minimum conditions. Water vapor and nitrogen monoxide are of special importance for UBAIM and present no important diurnal variations. The H_2O vmr decreases slowly above 95 km (Figure 1) because of the upward flux due to molecular diffusion: if this process was neglected, the abundance of water vapor would be smaller by one order of magnitude at 110 km *log-p* altitude.

[26] The distribution of NO at solstice (Figure 2) is in satisfactory agreement with the corresponding HALOE observations [*Siskind and Russell*, 1996]. As expected, the high concentrations of NO are confined to the lower thermosphere, except in the polar night. In this region, the absence of photolysis allows NO to be transported by the residual circulation down to the lower mesosphere.

2.2. Direct Solar Flux

[27] We use the solar photon flux from the SOLAR2000 model (Version 1.20) [*Tobiska et al.*, 2000] to calculate the photoionization rates of N_2, O_2, and O due to direct soft X-ray and EUV radiation. This model takes into account soft X-ray measurements by the SNOE satellite [*Solomon et al.*, 2001], which show a higher irradiance in this spectral region than earlier solar flux models [*Hinteregger et al.*, 1981] by a factor of 4. Absorption/ionization cross sections based on scattering factors from [*Henke et al.*, 1993], averaged in 1 nm bins, are used in the soft X-ray (1–10 nm) region. In the wavelength range from 10 to 103 nm, cross sections published by *Tohmatsu and Ogawa* [1990] are used. The SOLAR2000 model also provides the (direct) Lyman α intensity, which contributes to the ion production by ionizing NO. Secondary ionization by energetic photoelectrons is also included in the UBAIM in the local approximation (for a detailed description, see *Kazil* [2002] and references therein).

[28] In the wavelength range under consideration, mostly soft X-rays (1 nm < λ < 10 nm), selected lines of the EUV spectrum (HeII at 30.4 nm, CIII at 97.7 nm, Lyman β) and the Lyman α line dominate the photoionization in the lower thermosphere and upper mesosphere. Other bright lines (HeI 58.4 nm) are located in a region of the spectrum where atmospheric attenuation is large or lie outside of the energy range for ionization of the main atmospheric constituents (OIV at 103.2 and 103.8 nm).

[29] Hard X-rays (λ < 1 nm) are not a principal source of ionization in the lower ionosphere under quiet solar conditions. During solar flares, however, their intensity may increase by several orders of magnitude [*Brasseur and Solomon*, 1992], and their contribution to the ionization may exceed that of Lyman α [*Tohmatsu and Ogawa*, 1990]. Solar flare effects are not considered in this study, which addresses only undisturbed conditions.

[30] The ionization threshold of $O_2(^1\Delta_g)$ is 111.8 nm, which allows the ionization by the solar SiIII multiplet. This multiplet is located close to a deep atmospheric absorption minimum at 110.8 nm. As described above, the abundance of this excited neutral species is provided by the latest version of the SOCRATES model. We use the expression derived by *Paulsen et al.* [1972] that gives the O_2^+ produc-

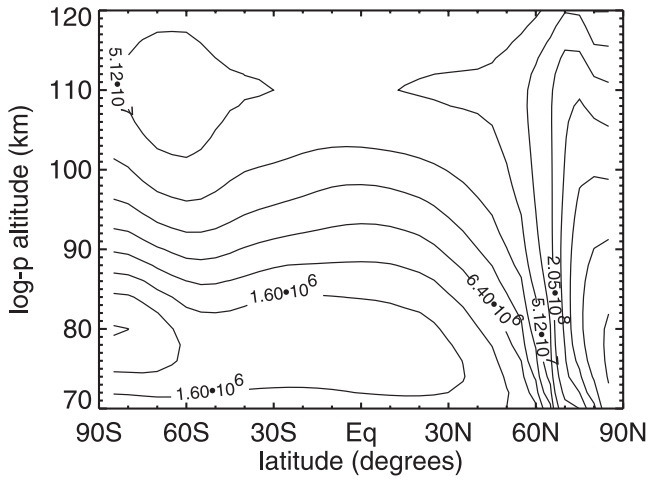

Figure 2. NO number density (cm^{-3}), 1996-12-21, 1200, computed by SOCRATES. Contour step is a factor of 2.

tion from $O_2(^1\Delta_g)$ as function of the $O_2(^1\Delta_g)$ abundance and of the O_2 column density.

2.3. Scattered Solar Flux

[31] While line-center fluxes are negligible compared with the direct line-integrated solar fluxes entering the atmosphere over much of the dayside of the Earth, multiple scattering of Lyman line emissions within the optically thick atomic hydrogen density distribution maintains appreciable fluxes of both Lyman α and Lyman β throughout the night. The atomic hydrogen density distribution peaks in the mesosphere with values in the range $\sim(1-4) \cdot 10^8$ cm^{-3} near 85 km altitude and extends out to beyond 10 R_E.

[32] Photoionization of NO and O_2 by resonantly scattered solar Lyman α and Lyman β, respectively, is modeled in the UBAIM using global spherically integrated fluxes calculated with the **lyao_rt** ("Lyman Alpha-Omega Radiative Transport") code of *Bishop* [1999, 2001]. **lyao_rt** results are shown in Figure 3. The spherical fluxes presented by *Strobel et al.* [1974] and used in earlier nightside ionosphere models were based on isothermal radiative transport calculations employing artificial "black layers" near 100 km altitude to account for O_2 photoabsorption and hence are not suitable for D-region applications.

[33] In **lyao_rt** the atomic hydrogen density profile [H](z) at a selected latitude and longitude is specified using five parameters to cover the entire $70 - 2 \cdot 10^5$ km altitude range. In the current study these are [H] at the mesospheric peak near 85 km, provided by SOCRATES; [H] at a reference upper thermospheric altitude (474 km for Lyman α, 492 km for Lyman β) provided by MSISE-90 [*Hedin*, 1991]; the net (total) upward diffusive flux generated by MLT photochemistry; and two parameters for characterizing the satellite atom component consistent with the [H] and exobase temperature variations established by the adopted thermospheric model [*Bishop*, 1991]. (At the altitudes of interest, specifics regarding the satellite population have little impact so long as a good estimate of the total geocoronal content is provided.) Solar minimum line-center fluxes of $3 \cdot 10^{11}$ ph cm^{-2} s^{-1} Å^{-1} for Lyman α and $5 \cdot 10^9$ ph cm^{-2} s^{-1} Å^{-1} for Lyman β [*Warren et al.*, 1998] have been adopted.

[34] In this initial study, computation of the **lyao_rt** source functions for each latitude/longitude grid point on the dayside has been carried out assuming that the multiply scattered component is dominated by the conditions near the location of interest. Upon crossing the terminator, the source functions are estimated using the multiple scattering components established by the upper thermospheric and geocoronal ballistic (z) distributions in the region of the terminator crossings specified by the great circles connecting the latitude/longitude grid points to the subsolar point. While somewhat simplistic, this approach faithfully captures the dawn-dusk differences; near midnight, however, the approximation begins to break down, as shown by the differences in the near-midnight spherical fluxes in Figure 3.

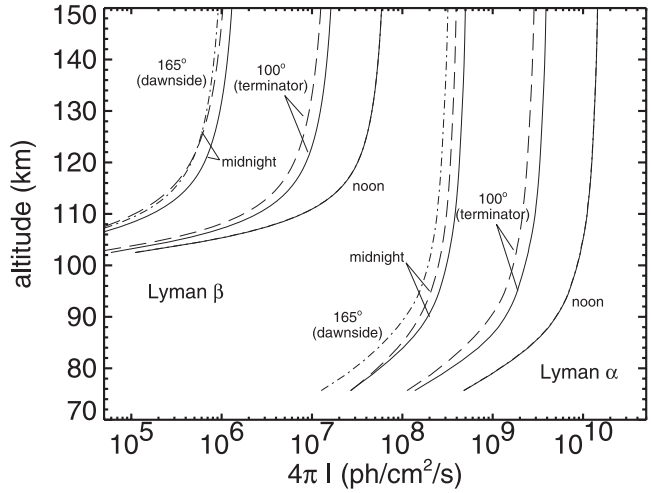

Figure 3. Spherically integrated fluxes of airglow Lyman α and Lyman β, 1996-12-21, 25°N, calculated by **lyao_rt**. Near-subsolar spherical fluxes show little or no variation in going from late morning to early afternoon ("noon" curves). As the terminator is approached, diurnal variations become more evident (at 100° SZA), with the larger fluxes on the dusk side (solid curves) owing mainly to the increased scattering optical depths on the dawn side at the altitudes of interest. For both Lyman α and Lyman β, the weakest spherical flux profiles (dot-dash curves) are located roughly 1 hour after local midnight (at 165° SZA) in the considered solar minimum/solstice conditions. A simplistic approximation has been used here for the nightside source functions in **lyao_rt**, leading to the differences shown for the near premidnight and postmidnight profiles (solid and dash curves, respectively).

2.4. Energetic Particles

2.4.1. Galactic Cosmic Rays

[35] Galactic cosmic rays (GCRs), primarily protons, penetrate to the Earth atmosphere and cause ionization. This ionization is more intense in the polar cap regions since, depending on the kinetic energy, GCRs are guided by the magnetic field lines. GCR ionization rates increase with the atmospheric density and thus with decreasing altitude, reaching a maximum between 10 and 15 km. Below $\sim$65 km, galactic cosmic rays are the dominant source of ionization. *Heaps* [1978] has derived a parametrization of the ion production rate due to cosmic rays as a function of (geomagnetic) latitude and solar activity. We use his expression, except that we do not account for the difference between geomagnetic and geographic coordinates.

2.4.2. Solar Cosmic Rays

[36] During large solar flares, charged particles (solar cosmic rays, SCR, also known as solar energetic particles, SEP) can be emitted from the surface of the Sun into space. This increased outflow may enhance the ionization in the Earth's atmosphere over several days by factors of 10^3 to 10^8 [*Brasseur and Solomon*, 1992]. Such events occur with a frequency that varies from approximately once every 2 months to once every 2 years [*Jursa*, 1985]. At present, we do not take these events into account.

2.4.3. Auroral Particles

[37] Precipitating particles (primarily electrons in the energy range of 1–20 keV) stored in the Earth's magnetosphere cause additional ionization along the magnetic field lines in the auroral ovals (mainly at altitudes from 90–150 km) and their equatorward neighboring regions,

the diffuse auroral zones. This source depends strongly on geomagnetic activity and changes quickly with time. In addition, Bremsstrahlung radiation (at 60–100 km) from auroral electron precipitation must be taken into account when computing auroral ionization rates. Introduction of these phenomena into the UBAIM has not yet been implemented.

2.5. Numerical Formulation

[38] The pivotal problem in the UBAIM is to solve numerically the stiff first-order system of differential equations

$$\dot{y} = f(y), \tag{1}$$

where y denotes the vector of ion number densities. In the course of the integration, $f(y)$ must be evaluated many times by the routine solving the system of differential equations. The set of equation (1) can be written as

$$\dot{y}_i = v_i + \sum_j \left(m_{ij} + r_{ij} \cdot y_i\right) \cdot y_j. \tag{2}$$

Here, v_i represents the initial electron/ion production rates, m_{ij} represents the (photo-) chemistry rates, and r_{ij} represents the recombination rates. The matrices $m_{i,j}$ and $r_{i,j}$ are sparse and the brute-force approach of calculating their elements one by one yields a longer runtime than if an efficient approach is chosen, which consists of jumping from one nonzero element to the next. The right-hand side of equation (2) is evaluated at every integration step, its coefficients v_i, m_{ij}, and r_{ij} are updated at every external timestep. We use Gear's backward differentiation formulae [*Gear*, 1969, 1971; *Jacobson*, 1999] for the numerical integration.

[39] We do not require our model results to fulfill the equilibrium criterion $dy(t)/dt = 0$, as the ions in the middle atmosphere in general are not in photochemical equilibrium. We rather iterate a single fixed day of year, starting with a small initial ion population, until we obtain a periodical solution for this day. We thus do not proceed from one day of year to the next but return at 2400 to 0000 of the same day. As the solar input and the background atmosphere are perfectly periodic in this case, we would expect the solutions of the system of differential equations to be periodic, too.

2.6. Mode of Operation

[40] The UBAIM covers the latitude range from 85°S to 85°N in steps of 5° and the log-pressure altitude range from 20 to 120 km. The start and end coordinates (latitude, altitude) are specified within these ranges, with the height or altitude grid interval specified in integer steps of at least 1 km. We use log-pressure altitudes where specified for reasons of consistency with the input from the SOCRATES model. The connection between geometric and *log-p* altitude is explained by *Chabrillat* [2001]. We merely note that this connection depends implicitly on latitude so that the geometric altitude cannot be displayed on the vertical axis of a latitude/altitude plot without first transforming the plotted function onto non-orthogonal coordinates.

[41] The year, the day of year, and the level of solar activity must be selected. Beginning with the southernmost latitude, the model loops through the latitudes of the integration area. At each latitude, the model goes through the altitudes of the integration area, starting with the lowermost. Column densities of N_2, O_2, and O, calculated with SOCRATES and MSISE-90, are used in determining the attenuation of the solar flux. The initial ionization due to direct solar X-rays, EUV and Lyman α, the secondary ionization due to energetic photoelectrons, and the ionization from scattered light are calculated and updated at every external timestep (5 min), as well as the background atmosphere taken from the SOCRATES model. Ionization from galactic cosmic rays is calculated by means of the expression given by *Heaps* [1978].

[42] The time step of the routine solving the system of differential equations is much shorter than the external timestep and is adjusted automatically, according to a chosen integration precision. At each integration step, the production and loss rates of the different species from ion chemistry, recombination, and photodetachment are updated, and a set of new densities is computed. The results are stored at an adjustable sampling rate but at least after every external timestep.

[43] The density of each charged species exceeding a certain threshold (0.1 cm^{-3}) is compared with that of the previous "day" or diurnal cycle. If the difference is less than an adjustable daily periodicity criterion (typically 0.5%) for each species, a periodical solution is assumed and integration commences at the next gridpoint. Species that do not exceed the threshold may exhibit periodic behavior or decay continuously.

[44] Below ~56 km, it typically takes two or three "days" or diurnal cycles until a periodical solution is reached. In the region between 56 and 84 km, where the ionization rate is low and ion lifetime long, up to seven "days" may be required. In rare cases it may happen that the periodicity criterion is not fulfilled within ten "days", in which case the criterion is doubled for the next ten "day" period. If at all, only rare species (<2 cm^{-3}) exhibit a bad convergence behavior.

[45] The UBAIM preserves charge neutrality up to 10^{-5}%, meaning that the number of uncancelled charges is less than 10^{-5}% of the dissociated pairs. In most parts of the integration area, charge conservation is better than this by orders of magnitude.

2.7. Ion Chemistry

[46] The important channels of the ion chemistry in the MLT region are discussed here. The rate coefficients from earlier model versions have been thoroughly reviewed and updated with more recent data. In certain cases, missing rate coefficients have been calculated by the methods of *Langevin* [1905] or *Chesnavich et al.* [1980], *Su and Chesnavich* [1982] and *Su* [1988]. In rare cases, rate coefficients had to be estimated by comparison with similar reactions. The entire set of 311 reactions and their rate coefficients for the 71 charged species comprised by the model are given and discussed by *Kazil* [2002], together with caveats emerging from uncertainties in these data.

2.7.1. Important Positive Ions and Channels

[47] The starting point for the positive ion chemistry are the reactions of O^+, O_2^+, N^+, N_2^+, and NO^+, which are

directly produced by sunlight and by energetic particles. N^+, N_2^+, and O^+ react with O_2 to produce O_2^+:

$$N^+ + O_2 \rightarrow N + O_2^+ \quad (3)$$

$$N_2^+ + O_2 \rightarrow N_2 + O_2^+ \quad (4)$$

$$O^+ + O_2 \rightarrow O + O_2^+ \quad (5)$$

NO^+ is also produced by means of the reactions

$$N^+ + O_2 \rightarrow NO^+ + O \quad (6)$$

$$N_2^+ + O \rightarrow NO^+ + N \quad (7)$$

$$N_2^+ + NO \rightarrow NO^+ + N_2 \quad (8)$$

$$O^+ + N_2 \rightarrow NO^+ + N \quad (9)$$

$$O_2^+ + NO \rightarrow NO^+ + O_2 \quad (10)$$

Thus above a transition height (located between 72 and 92 km, [*Kopp and Herrmann*, 1984]), O_2^+ and NO^+ are the dominant positive ion species. At the transition height the H_2O density is sufficiently large to allow the hydration of NO^+ in three-body collisions:

$$NO^+(H_2O)_n + H_2O + X \rightarrow NO^+(H_2O)_{n+1} + X \quad (11)$$

Below the transition height, the production of proton hydrates is initiated by the reactions

$$N^+ + H_2O \rightarrow H_2O^+ + N \quad (12)$$

$$N_2^+ + H_2O \rightarrow H_2O^+ + N_2 \quad (13)$$

$$O^+ + H_2O \rightarrow H_2O^+ + O \quad (14)$$

$$H_2O^+ + H_2O \rightarrow H^+(H_2O) + OH \quad (15)$$

$$H^+(H_2O)_n + H_2O + X \rightarrow H^+(H_2O)_{n+1} + X \quad (16)$$

At altitudes between roughly 65 and 75 km however, the formation of proton hydrates proceeds predominantly through the reaction

$$NO^+(H_2O)_3 + H_2O \rightarrow H^+(H_2O)_3 + HNO_2, \quad (17)$$

which depends on the ionization of NO by Lyman α. Below 65 km, Lyman α has mostly disappeared and O^+, N^+, and N_2^+ from GCR ionization enable the formation of proton hydrates in the reaction chain in equations (12)–(16).

[48] From laboratory studies a number of side channels leading to $H^+(H_2O)$ are known, for instance the reactions of H_2O^+ with CH_4 or H_2 [*Anicich*, 1993]. In previous versions of the UBAIM the reaction chain

$$O_2^+ + H_2O_2 \rightarrow H_2O_2^+ + O_2 \quad (18)$$

$$H_2O_2^+ + H_2O \rightarrow H^+(H_2O) + HO_2 \quad (19)$$

was a contributor of $H^+(H_2O)$ ions. Owing to the low H_2O_2 density, this scheme is much less effective than the one described above and is omitted in the present model version.

2.7.2. Important Negative Ions and Channels

[49] The starting point for the negative ion chemistry (below 80 km) is determined by three electron attachment reactions:

$$e + N_2 + O_2 \rightarrow O_2^- + N_2 \quad (20)$$

$$e + O_2 + O_2 \rightarrow O_2^- + O_2 \quad (21)$$

$$e + O_3 \rightarrow O^- + O_2 \quad (22)$$

The initial negative ions O^- and O_2^- react with CO_2, HNO_3, and HCl to form the core ions of the families with chlorinated, CO_3^-, and NO_3^- cores:

$$O^- + CO_2 + X \rightarrow CO_3^- + X \quad (23)$$

$$O^- + HNO_3 \rightarrow NO_3^- + OH \quad (24)$$

$$O^- + HCl \rightarrow Cl^- + OH \quad (25)$$

$$O_2^- + CO_2 + X \rightarrow CO_4^- + X \quad (26)$$

$$O_2^- + HNO_3 \rightarrow NO_3^- + HO_2 \quad (27)$$

$$O_2^- + HCl \rightarrow Cl^- + HO_2 \quad (28)$$

CO_4^- reacts with HCl to form $ClHO_2^-$ [*Dotan et al.*, 1978], a final species, with no known reactions with atmospheric tracers. NO_3^- undergoes three-body association reactions and forms cluster ions with H_2O, HCl, and HNO_3. CO_3^- forms clusters with H_2O as well as with HNO_3. The direct reactions with HNO_3 occur as well:

$$CO_3^- + HNO_3 \rightarrow HNO_4^- + CO_2 \quad (29)$$

$$CO_3^- + HNO_3 \rightarrow NO_3^- + CO_2 + OH \quad (30)$$

(after *Möhler and Arnold* [1991]). Cl^- forms clusters with H_2O and HCl and reacts with HNO_3 to form NO_3^-. An

experimentally not yet well established ion in the atmosphere [*Kopp*, 1992] is HCO_3^-, formed from OH^-:

$$OH^- + CO_2 + X \rightarrow HCO_3^- + X \quad (31)$$

In the sunlit mesosphere, electrons are detached from negative ions in a number of reactions, mainly by photodetachment

$$h\nu + J^- \rightarrow J + e \quad (32)$$

with $J^- = O^-, O_2^-, O_3^-, CO_3^-, \ldots$ and by associative electron detachment,

$$J^- + M \rightarrow M' + e \quad (33)$$

where M is one of O, $O_2(^1\Delta_g)$, and H. The released electrons recombine faster with positive ions than negative ions and thus reduce positive ion lifetimes during daytime.

[50] Atomic oxygen in the mesosphere is produced by ozone dissociation and appears short after sunrise in considerable amounts. *Turco and Sechrist* [1972c] concluded that this process is responsible for the increase of electron density after sunrise through the reaction $NO_3^- + O \rightarrow NO_2 + O_2^-$ and subsequent photodetachment, as opposed to immediate photodetachment from NO_3^-. However, their model involved various uncertainties in the rate coefficients, which have still not yet been resolved.

3. Selected Results

[51] We focus only on a few species here, in particular on diurnal variations of $NO^+(H_2O)$ for two reasons: First, positive ion chemistry in the upper mesosphere/lower thermosphere is considered to be much better understood than positive ion chemistry of lower atmospheric regions or negative ion chemistry in general. Negative ion chemistry is burdened with various uncertainties, particularly with respect to electron detachment, that heavily influence the resulting diurnal cycles. Second, $NO^+(H_2O)$ exhibits an interesting diurnal cycle stemming from the EUV absorption characteristics of the atmosphere, which thus can be expected to be less sensitive to uncertainties in reaction rate coefficients or neutral composition. Other positive ions with well known chemistry, such as O^+ and O_2^+, have comparatively trivial diurnal cycles, which essentially reflect the diurnal change of solar elevation.

[52] The $NO^+(H_2O)$ densities were computed for winter soltice 1996, under solar minimum conditions. Model results for August 12, 1976, are compared with rocket mass spectrometer measurements obtained on that date. Finally, UBAIM results are compared with ion densities in photochemical equilibrium.

3.1. $NO^+(H_2O)$

[53] Water clusters of NO^+ occur mainly in the upper mesosphere/lower thermosphere (Figure 4) because of the favorable coincidence of sufficient NO^+ production, low temperatures, and sufficiently abundant water vapor. These clusters cannot appear below a certain altitude (~75 km at the subsolar point) due to the absorption of Lyman α radiation by molecular oxygen. On the other hand, they cannot appear in high abundances above a certain altitude because of higher temperatures, low pressure, low water vapor abundance and depletion by free electrons. Figure 4 shows three local maxima in the $NO^+(H_2O)$ layer. Several factors contribute to the southern peak being located at a higher altitude than the northern peak at 50°N: The water vapor distribution extends to higher altitudes at 70°S than at 50°N (see Figure 1); in addition, below the southern summer peak, $NO^+(H_2O)$ is transformed to $NO^+(H_2O)_{n>1}$ as a result of the very low temperatures of the polar summer mesopause.

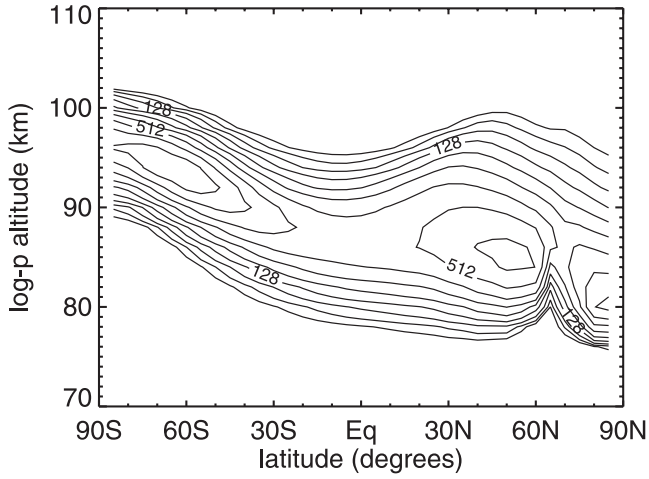

Figure 4. $NO^+(H_2O)$ number density (cm^{-3}), 1996-12-21, 1200. Contour step is a factor of $\sqrt{2}$. The maximum density is 1400 cm^{-3}.

[54] NO is less abundant around the equator in the lower thermosphere/upper mesosphere (see Figure 2), which accounts for the low density of $NO^+(H_2O)$ at low latitudes. In addition, EUV radiation at low solar zenith angles generates relatively large electron densities, removing $NO^+(H_2O)$ by recombination. The peak in the polar night (65–85°N) is caused by scattered Lyman α ionizing the persistent polar night NO population.

[55] Figure 5 shows the diurnal evolution of $NO^+(H_2O)$ at 98 km *log-p* altitude (located around 94.3 km geometric altitude). The dominant features here are the two peaks along the morning/evening terminator at low and middle latitudes. At noon we find a pronounced minimum in the equatorial region. Interestingly, at this altitude, the highest $NO^+(H_2O)$ concentrations can be found in the polar day around 2400. A night minimum occurs in the low northern latitudes between 0200 and 0300.

[56] Figure 6 shows four sections through the density distribution of Figure 5 at different latitudes. The curves bend sharply at sunrise and the density increases quickly, as direct Lyman α takes over from scattered Lyman α. The time-lag between the morning and the evening peak obviously depends on the day length. The curves are not symmetric in time: $NO^+(H_2O)$ is depleted mainly by recombination with electrons, which, in the evening, disappear along with the EUV radiation. The reduced electron density explains the shape of the curves after sunset, which is governed by a slow decrease and which clearly differs from the curve shape around sunrise. Additional asymmetry is caused by the fact that the scattered Lyman α flux is

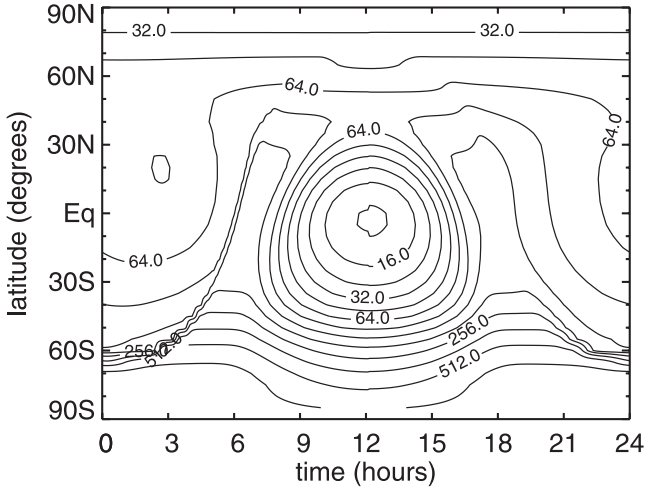

Figure 5. $NO^+(H_2O)$ number density (cm^{-3}), 1996-12-21, 98 km *log-p* altitude. Contour step is a factor of $\sqrt{2}$. The maximum density is 900 cm^{-3}.

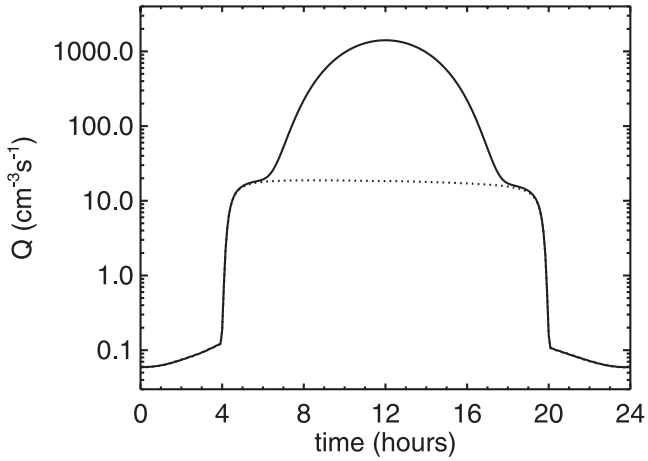

Figure 7. Diurnal variations of the production rate Q of electrons (solid line) and NO^+ (dotted line), 1996-12-21, 45°S, 98 km *log-p* altitude.

lowest about 1 h after local midnight, as seen in Figure 3. Thus the $NO^+(H_2O)$ night minimum is shifted dawnward.

[57] Figure 7 displays the reason for the $NO^+(H_2O)$ diurnal cycles: the production rate of NO^+, $Q(NO^+)$, and the production rate of electrons, Q(e), have different diurnal variations. In the mesospheric night, both production rates are due to scattered Lyman α. At sunrise, direct solar Lyman α, being only weakly absorbed, appears quickly: $Q(NO^+)$ increases suddenly, remains roughly constant during the day, and decreases suddenly at sunset. On the other hand, the EUV contribution to daytime Q(e) depends heavily on the solar zenith angle. Around noon, the electron production increases to considerable values, greatly surpassing the NO^+ production from Lyman α.

[58] Hence a morning peak in the $NO^+(H_2O)$ density emerges, when $Q(NO^+)$ is already strong, but the total electron density is still relatively low. Around noon the large electron population reduces the lifetime of $NO^+(H_2O)$ substantially through recombination and the $NO^+(H_2O)$ density reaches a minimum. A similar peak appears in the evening, when the electron density decreases faster than the supply of NO^+. The NO^+ diurnal cycle, however, does not exhibit these peaks, but has a noon maximum.

[59] Figure 8 shows snapshots of the altitude profile of $NO^+(H_2O)$ at different times of day. At 0000 the $NO^+(H_2O)$ layer is located around 96 km. As time progresses, the layer seems to descend, while its peak density increases. The spatial displacement of the layer is, however, not a transport phenomenon. It can be explained by the differing absorption characteristics for Lyman α and EUV radiation in the atmosphere: At night, scattered Lyman α maintains a low ionization rate at altitudes down to roughly 85 km, see Figures 3 and 8. In the course of the day the increasing penetration of direct Lyman α is capable of ionizing NO at lower altitudes, and the $NO^+(H_2O)$ layer forms at 85 km. At higher altitudes, however, the resulting $NO^+(H_2O)$ clusters are efficiently depleted by solar EUV-generated electrons.

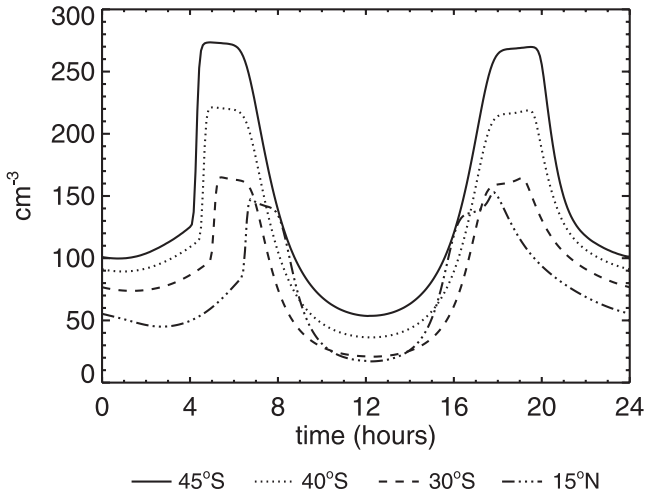

Figure 6. Diurnal variations of the $NO^+(H_2O)$ number density at selected latitudes, 1996-12-21, 98 km *log-p* altitude.

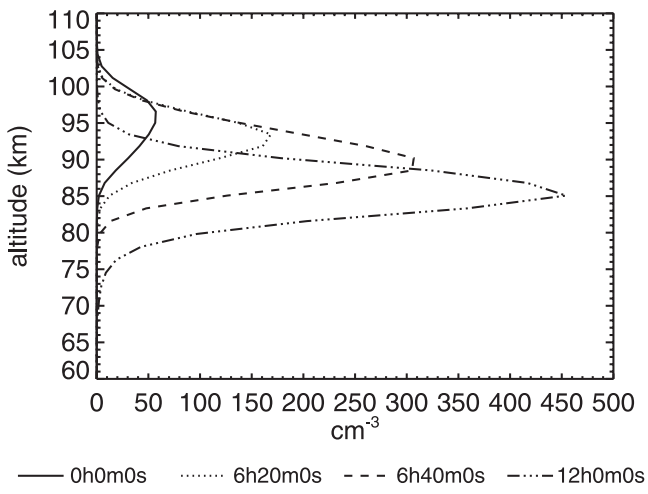

Figure 8. Altitude profiles of the $NO^+(H_2O)$ number density at different times of the day between midnight and noon, 1996-12-21, at the equator.

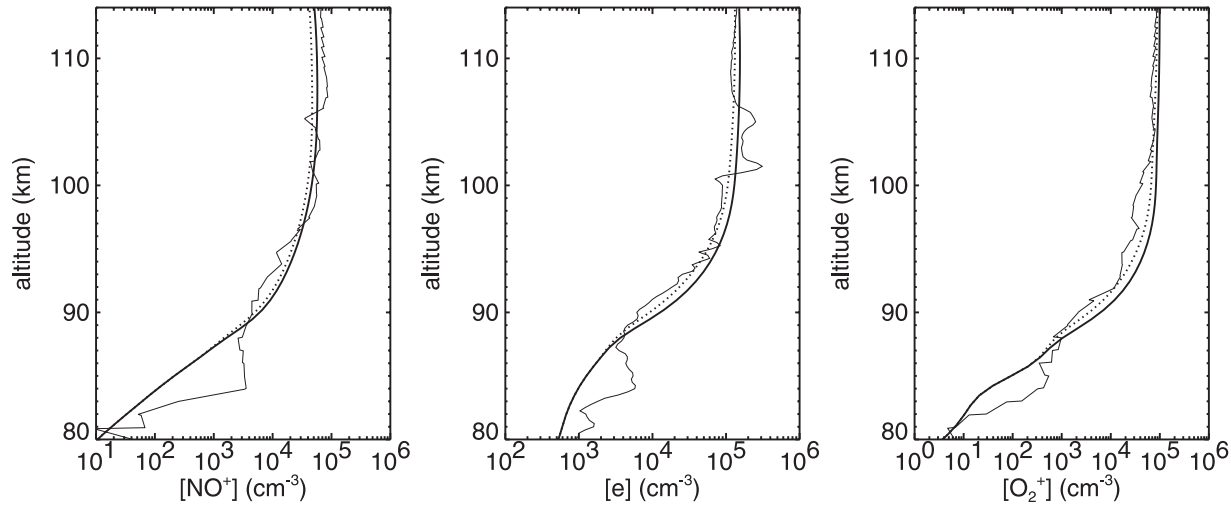

Figure 9. Comparison between UBAIM results and observations, both for 12 August 1976, 1054: UBAIM results at 40°N (thick curves), UBAIM results for the same latitude, but with soft X-ray flux reduced by a factor of 0.5 (dotted curves), and measurements by *Herrmann et al.* [1978] over Wallops Island at 37.8°N (thin curves).

Only in the region where Lyman α is strong and EUV weak can a considerable number of these clusters survive.

3.1.1. Sensitivity Studies of the Dawn and Dusk Peaks

[60] In order to test to what extent the existence of the morning/evening peaks in the $NO^+(H_2O)$ density are affected by uncertainties in the model parameters, we performed a series of sensitivity studies. First, we (independently) changed the NO and H_2O density by factors of 3 and 1/3. These variations only mildly influence the dawn and dusk peaks of $NO^+(H_2O)$. While higher H_2O or NO densities result in smaller peak/valley ratios and a shift in baseline altitude for the diurnal cycle of $NO^+(H_2O)$, the morning and evening peaks remain distinctly present in all four cases.

[61] In a second series of sensitivity tests, we varied the rate coefficient for the reaction

$$NO^+(H_2O) + e \rightarrow M + M' \qquad (34)$$

by factors of 1.5 and 0.5. This rate coefficient is known only from comparison with similar reactions and amounts to $1.5 \cdot 10^{-6}\left(\frac{300K}{T}\right)^{1/2}$ cm^{-3} s^{-1} in our model. The temperature dependence of $T^{-1/2}$ has been introduced by *Bardsley and Biondi* [1970] for this kind of reactions.

[62] Variations in the rate of the reaction in equation (34) have an almost reciprocal effect on the $NO^+(H_2O)$ abundance. Even in the most unfavorable case, where the recombination rate has been increased by a factor of 1.5, the morning and evening peaks remain clearly visible with a peak/valley ratio remaining close to 6.

3.2. Comparison of UBAIM Results With Observations

[63] For comparison with observations we use data obtained from a rocket flight performed at Wallops Island (37.8°N) on 12 August 1976 under quiet geomagnetic conditions, at 1054 local time [*Herrmann et al.*, 1978; *Kopp et al.*, 1978]. Model results were calculated for this date and local time for the latitude of 40°N. The disagreements between the model and these observations will be discussed in section 4.

[64] Figure 9 shows the electron, O_2^+, and NO^+ densities measured by *Herrmann et al.* [1978] and the corresponding UBAIM results. The peaks near 103 km in the measured electron density are caused by a sporadic E-layer. Model results and NO^+ observations agree well above 90 km, with occasional deviations in both directions. Below 90 km the model clearly underestimates the NO^+ population, at 83 km by more than a factor of 10. Similar deviations in the electron and O_2^+ density occur in the same altitude region. Above 90 km the model results for these species are much closer to observations, although overestimating them in general.

[65] Figure 10 compares UBAIM profiles of the proton hydrates $H^+(H_2O)_{n=2,3,4}$ with corresponding observations by *Kopp et al.* [1978] from the campaign mentioned above. The UBAIM $H^+(H_2O)_2$ density is systematically too low. Significant disagreement occurs in the $H^+(H_2O)_3$ density, where observations surpass the model results by more than one order of magnitude, except around 86 km. The UBAIM $H^+(H_2O)_4$ density agrees well with observations below 86.5 km but decreases much faster with altitude above this level than the observed values.

[66] Figure 11 shows the UBAIM $NO^+(H_2O)$ altitude profile and the observed $NO^+(H_2O)$ profile acquired by *Kopp et al.* [1978]. The model reproduces the altitude distribution of the $NO^+(H_2O)$ layer quite accurately but overestimates its center density. In addition, observed $NO^+(H_2O)$ values notedly exceed the model results above 94 km.

3.3. Comparison With the Equilibrium Approach

[67] A common approach in implementing models of ion chemistry is to assume that the ions can be treated as in photochemical equilibrium and to set the left-hand side of equation (2) to zero. The resulting equation can be solved by iteration, provided that the iteration converges to a fixed point. This approach works particularly well in regions where ion lifetimes are short and if efficiently implemented, may result in shorter runtimes than the numerical integration employed in the UBAIM.

[68] We implement another method to obtain such a fixed point solution by slightly modifying our model code: We integrate equation (2) numerically for each time step of a

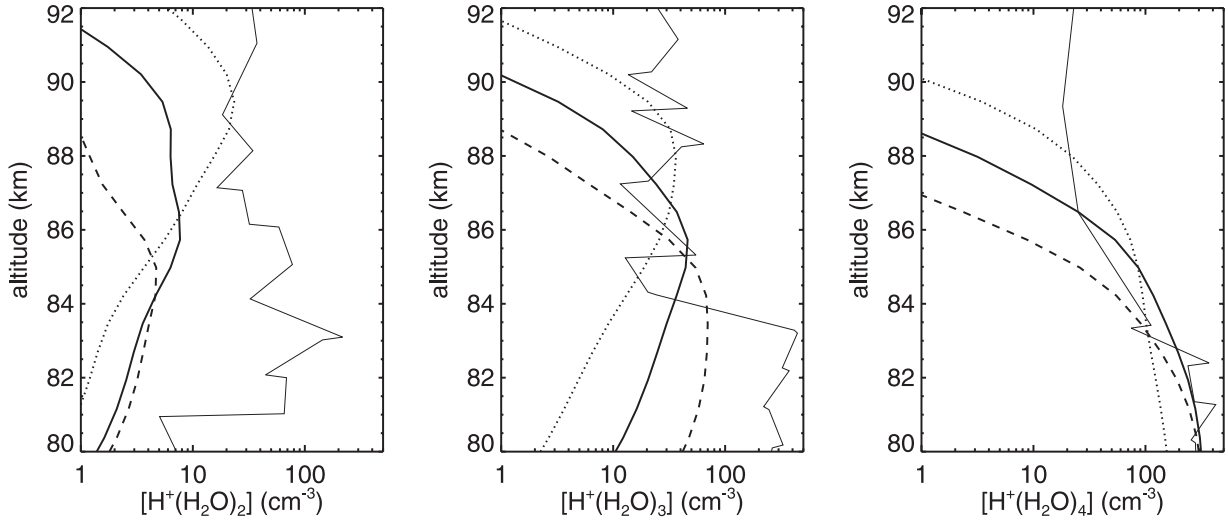

Figure 10. Comparison between UBAIM results and observations, both for 12 August 1976, 1054: UBAIM results at 40°N (thick curves), UBAIM results for the same latitude but with water vapor increased by a factor of 5 (dotted curves), reduced by a factor of 1/5 (dashed curves), and measurements by *Kopp et al.* [1978] over Wallops Island at 37.8°N (thin curves).

day with fixed coefficients v_i, $m_{i,j}$ and $r_{i,j}$ until the change in the ion densities falls below a certain limit (0.001%/300 s). In other words, we "freeze" the physical parameters (solar flux, neutral composition, etc.) at each time step and let the numerical integration proceed until the ion densities are close to photochemical equilibrium. We then continue with the next time step (adjusting the coefficients v_i, $m_{i,j}$ and $r_{i,j}$ accordingly), using the densities of the previous time step as initial values. The resulting diurnal cycles can be considered in photochemical equilibrium.

[69] Figure 12 shows a comparison of UBAIM and equilibrium dissociated pair densities at 69 km. The equilibrium curve peaks exactly at 1200, whereas the peak in the UBAIM curve is shifted by 2 hours into the afternoon. This delay reflects the overall timescale of ion chemistry at this altitude, as the effect of the ionizing radiation (Lyman α) on the initial species has to propagate through the complex chemical scheme before reaching the final species. The equilibrium peak is higher by roughly 20% than the UBAIM peak because the photochemical system in the "real" atmosphere has not had sufficient time to approach equilibrium before the Sun passes its maximum elevation.

[70] The edge in the UBAIM curve at sunrise in Figure 12 is caused by photodetachment of electrons from negative ions. These electrons deplete the positive ions and thus reduce the number of dissociated pairs. The photodetachment rates used in the UBAIM are subject to substantial uncertainties and the resulting morning depletion of the charged species must be considered with caution. This does not, however, affect the comparison in Figure 12 because the same rates are used in both cases. Thus the morning depletion can also be seen in the equilibrium curve, followed by a small local peak of unidentified origin.

[71] In the afternoon the equilibrium curve quickly falls as the ion densities adjust to the local decreased Lyman α intesities. The low values before sunset are again due to photodetachment. The constant nighttime abundance is maintained solely by GCR ionization, since at this altitude scattered Lyman α fluxes are too attenuated to have an impact. In contrast, the UBAIM curve exhibits a slower decrease which is due to the long lifetimes of the final species. The ion lifetimes are so long at this altitude that ions produced in the late afternoon can survive even until sunrise, which explains why the UBAIM curve never reaches the nighttime GCR equilibrium value.

4. Discussion

[72] The comparison of UBAIM results and observations shows partial agreement, revealing the difficulties in reproducing experimental data. In this respect, the UBAIM has several fundamental limitations common to all ion models of the MLT region, even if properly implemented. One of

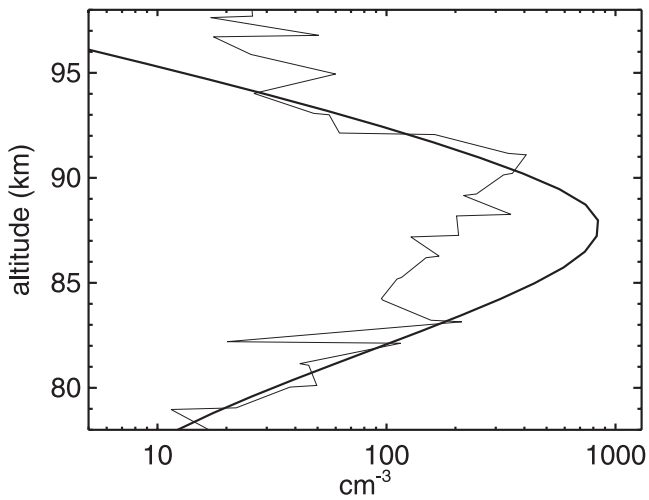

Figure 11. Comparison between UBAIM $NO^+(H_2O)$ at 40°N (thick curve), and measurements by *Kopp et al.* [1978] over Wallops Island at 37.8°N (thin curve), both for 12 August 1976, 1054.

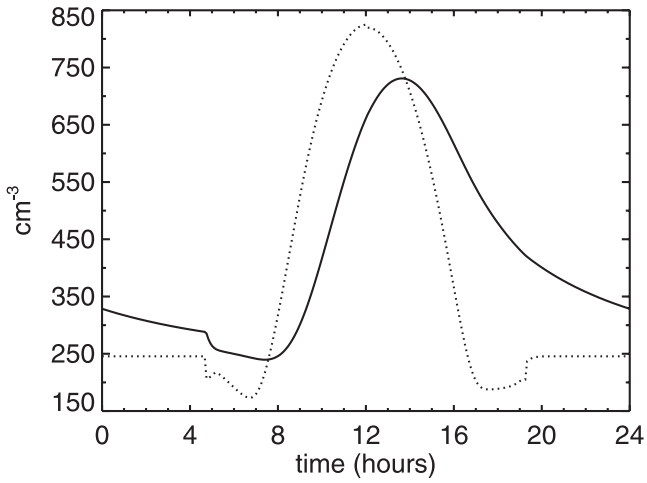

Figure 12. Comparison of UBAIM diurnal variations of the dissociated pair density (solid line) with results in photochemical equilibrium (dotted line), 20°S, 1996-12-21, 69 km altitude.

these involves the highly variable conditions in this atmospheric region, which alter the ion composition through short timescale changes in neutral composition, temperature, energetic particles and X-rays. Our background atmosphere and ionization sources do not account for variations in these quantities on short timescales (minutes to tens of minutes). On the other hand, uncertainties in measured reaction rate coefficients compromise the capabilities of ion models to reproduce observations: as an example, we point to the compilation by *Ikezoe et al.* [1987], which gives a very large number of rate coefficients for ion-molecule reactions. A quick glance reveals that the error estimates in these data frequently amount to 30%, and larger errors are not difficult to find.

[73] It is difficult to identify unambiguously the reasons for the disagreement seen in Figures 9, 10, and 11. However, some details are worth discussing. We have seen that between 80 and 90 km the model underestimates the densities of the initial charged species (Figure 9). This cannot be due to a local NO peak at the time of the measurement, as this would not explain the high O_2^+ density. Notional explanations include precipitating particles, increasing the ion production locally, or an increased lifetime of the positive ions due to the occurrence of immobile negative species. The electron density presented in Figure 9 has not been measured directly but determined as the sum of positive species. However, the occurrence of negative species with a lower recombination rate than electrons at this altitude, latitude, and time of day is highly speculative.

[74] Between 90 and 100 km the model tends to overestimate the electron and O_2^+ population. This may be due to an overestimation of the the ionization rates in the region in question. It is tempting to assume that the disagreement is linked to wavelengths subject to strong variations, such as X-rays. Recent measurements by the SEE instrument on board of the TIMED satellite show that soft X-rays (1–10 nm) vary on timescales of one solar rotation by a factor between 1.4 and 2. In addition, both SNOE and SOLAR2000 overestimate the soft X-ray flux by a factor of roughly 1.3 (S. C. Solomon, personal communication, 2003). Indeed, a reduction of the flux by a factor of two in this wavelength region brings UBAIM results and observations in good agreement (see Figure 9).

[75] More complex mechanisms are likely responsible for the disagreement of modeled and observed proton hydrate distribution (Figure 10): The agreement of the $H^+(H_2O)_4$ results below 86.5 km contrasts with the disagreement of $H^+(H_2O)_2$ and $H^+(H_2O)_3$ in the same altitude region. Above 87 km the model underestimates all three species. This is unlikely due to systematically higher water vapor mixing ratios during the measurement: A sensitivity test with H_2O increased by a factor of 5 does not lead to systematically higher $H^+(H_2O)_{n=2,3,4}$ abundances (see Figure 10): This is the case only above roughly 86 km. Below this altitude, higher water vapor densities reduce these proton hydrates. A uniform reduction of the H_2O density by a factor of 1/5 improves the agreement only in the case of $H^+(H_2O)_3$ below 85 km. Thus an unlikely high water vapor abundance confined to altitudes above 86 km would be required to bring the model results in agreement with the data. Below this altitude, variations of water vapor alone seem not to be sufficient to reproduce observations.

[76] Cluster formation depends strongly on temperature, and temperature deviations from the adopted MSIS temperature may result in significantly different proton hydrate profiles. Considerable temperature variations occur in the upper mesosphere [*Lübken et al.*, 1999; *Preusse et al.*, 2001], and may be another factor related to the disagreement of the model results and observations.

[77] An alternative explanation for the high mass 55 signal above 87 km (Figure 10), interpreted as $H^+(H_2O)_3$, is $^{55}_{25}Mn^+$ from meteoric ablation. Similarly, the high $H^+(H_2O)_4$ abundance above 87 km may be a result of the contamination of the 73 amu mass spectrometer channel by $NO^+(CO_2)$ with a mass of 74 amu (Figure 13).

[78] In the higher-altitude cases (Figures 9–11) we do not attribute the data-model disagreements to the neglect of

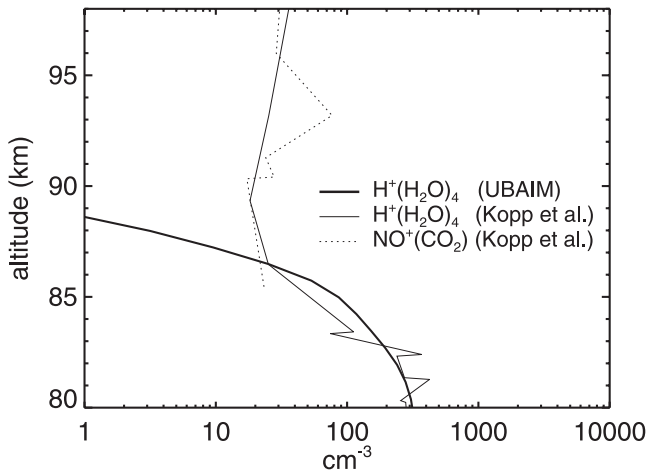

Figure 13. UBAIM $H^+(H_2O)_4$ profile at 40°N, and data from *Kopp et al.* [1978] over Wallops Island at 37.8°N, both for 12 August 1976, 1054. The $H^+(H_2O)_4$ (73 amu) mass spectrometer channel is likely contaminated by $NO^+(CO_2)$ (74 amu) above 86 km.

vertical transport in the UBAIM, given the brief photochemical lifetimes at the locations and times in question (less than 40 s for the ions and less than 4 min for electrons).

[79] At lower altitudes (69 km, see Figure 12), comparison of the UBAIM and equilibrium results clearly shows that photochemical equilibrium does not apply, with the average lifetime of the most abundant negative ion exceeding ~6 hours. Thus the UBAIM results in this altitude region may be hampered by the neglect of vertical transport.

[80] At higher altitudes, higher ionization rates during daytime shorten ion lifetimes sufficiently so that the equilibrium approach is appropriate. At lower altitudes, it is legitimate to assume photochemical equilibrium as well, owing to the absence of diurnal cycles in the ion-chemical forcing. However, during and after episodes of quickly changing ionization, e.g., due to auroral electron precipitation or solar cosmic rays events, nonequilibrium effects can be expected. In addition, under solar maximum conditions, GCR ionization is less intense, and Lyman α penetrates deeper into the mesosphere. A shift of the altitude range where nonequilibrium conditions govern the background (undisturbed) ion population can be expected.

5. Summary and Conclusions

[81] We introduce the University of Bern Atmospheric Ion Model (UBAIM version 5.25). This model constitutes a major step forward in the development of atmospheric ion models, as for the first time, a time-dependent model of the MLT ion chemistry is used in conjunction with a time-dependent 2-D model of the neutral atmosphere. Updated results for dayside solar irradiance and nightside scattered Lyman α and β fluxes are used in calculating the driving photoionization rates. Diurnal cycles of $NO^+(H_2O)$ in the MLT region, showing nontrivial behavior, are presented and discussed. Model results are compared both with solar minimum rocket flight data [*Herrmann et al.*, 1978; *Kopp et al.*, 1978] and with photochemical equilibrium model results.

[82] The model is in fair agreement with certain observations and fails to reproduce others. This may stem, at least in part, from the undisturbed, climatically averaged model atmosphere conditions adopted in the current modeling. Ambiguity with respect to the identification of certain charged species by mass spectrometers is another difficulty. Averaging the solar flux and absorption/ionization cross sections over 1 nm bins, instead of folding cross sections with line profiles, possibly introduces additional bias. However, the main limitation may lie in the substantial uncertainties in a number of reaction rate coefficients and the currently limited knowledge of relevant ion chemical reaction paths, which become increasingly important at decreasing altitudes.

[83] In addition to these intrinsic difficulties, more general problems affect the comparison of ion model results with observations. Rocket and balloon campaigns were the major sources of data for validation of ion models. Covering only small segments of space and time or focusing on very particular phenomena, they do not provide a representative picture of atmospheric ion composition and its variability. They slowly went out of fashion in the past decade with the rise of remote sensing satellites. Hence the database for ion model validation is rather sparse, as opposed to validation of neutral models, where data with global coverage and often for long periods of time are available.

[84] Ion modeling is therefore confronted with various fundamental problems. Despite these problems, the UBAIM allowed the prediction of previously unrecognized phenomena (e.g., $NO^+(H_2O)$ diurnal variations), assessment of their persistence and response to varying conditions, and investigation of where ion species vertical transport may be important. The formation of aerosol particles and of polar stratospheric and polar mesospheric clouds are areas of current atmospheric research. The contribution from processes such as ion-induced nucleation or cluster formation from ion recombination is at best unclear. Further development of ion models is necessary to clarify their significance. However, more experimental work in the field is needed to provide input and validation data for ion models.

[85] **Acknowledgments.** This work is supported by the Swiss National Science Foundation. Support for Simon Chabrillat was provided by projects "MO/35/002" and "BASCOE (Prodex)" funded by the SSTC/DWTC service of the Belgian Government. Support for James Bishop was provided by the Office of Naval Research. We wish to thank Etienne Arijs and Gaston Kockarts (Belgian Institute for Space Aeronomy, Brussels) and Guy Brasseur (Max Planck Institute for Meteorology, Hamburg) for helpful discussions. The reviewers of this paper provided valuable comments. SOLAR2000 Research Grade historical irradiances were provided courtesy of W. Kent Tobiska and SpaceWx.com. These historical irradiances have been developed with funding from the NASA UARS, TIMED, and SOHO missions.

References

Anicich, V. G., Evaluated bimolecular ion-molecule gas phase kinetics of positive ions for use in modeling planetary atmospheres, cometary comae, and interstellar clouds, *J. Phys. Chem. Ref. Data*, *22*, 1469–1569, 1993.

Arijs, E., and G. P. Brasseur, Acetonitrile in the stratosphere and implications for positive ion composition, *J. Geophys. Res.*, *91*, 4003–4016, 1986.

Arijs, E., D. Nevejans, and J. Ingels, Unambiguous mass determination of major stratospheric positive ions, *Nature*, *288*, 684–686, 1980.

Arijs, E., D. Nevejans, P. Frederick, and J. Ingels, Stratospheric positive ion composition measurements, ion abundances and related trace gas detection, *J. Atmos. Terr. Phys.*, *44*, 43–53, 1982a.

Arijs, E., D. Nevejans, P. Frederick, and J. Ingels, Stratospheric negative ion composition measurements, ion abundances and related trace gas detection, *J. Atmos. Terr. Phys.*, *44*, 681–694, 1982b.

Arijs, E., D. Nevejans, J. Ingels, and P. Frederick, Negative ion composition and sulfuric acid vapour in the upper stratosphere, *Planet. Space Sci.*, *31*, 1459–1464, 1983.

Arnold, F., and D. Krankowsky, Negative ions in the lower ionosphere: A comparison of a model computation and a mass-spectrometric measurement, *J. Atmos. Terr. Phys.*, *33*, 1693–1702, 1971.

Arnold, F., J. Kissel, D. Krankowsky, H. Wieder, and J. Zähringer, Negative ions in the lower ionosphere: A mass-spectrometric measurement, *J. Atmos. Terr. Phys.*, *33*, 1169–1175, 1971.

Arnold, F., R. Fabian, E. E. Ferguson, and W. Joos, Mass spectrometric measurements of fractional ion abundances in the stratosphere—Negative ions, *Planet. Space Sci.*, *29*, 195–203, 1981.

Bardsley, J. N., and M. A. Biondi, Dissociative recombination, *Adv. At. Mol. Phys.*, *6*, 1–57, 1970.

Beig, G., S. Walters, and G. P. Brasseur, A two-dimensional model of ion composition in the stratosphere: 1. Positive ions, *J. Geophys. Res.*, *98*, 12,767–12,773, 1993a.

Beig, G., S. Walters, and G. P. Brasseur, A two-dimensional model of ion composition in the stratosphere: 2. Negative ions, *J. Geophys. Res.*, *98*, 12,775–12,781, 1993b.

Berger, U., and U. von Zahn, The two-level structure of the mesopause: A model study, *J. Geophys. Res.*, *104*, 22,083–22,093, 1999.

Bishop, J., Analytic exosphere models for geocoronal applications, *Planet. Space Sci.*, *39*, 885–893, 1991.

Bishop, J., Transport of resonant atomic hydrogen emissions in the thermosphere and geocorona: Model description and applications, *J. Quant. Spectrosc. Radiat. Transfer*, *61*, 473–491, 1999.

Bishop, J., Thermospheric atomic hydrogen densities and fluxes from dayside Lyman α measurements, *J. Atmos. Sol. Terr. Phys.*, *63*, 331–340, 2001.

Brasseur, G. P., and A. Chatel, Modelling of stratospheric ions: a first attempt, *Ann. Geophys.*, *1*, 173–185, 1983.

Brasseur, G. P., and P. De Baets, Ions in the mesosphere and lower thermosphere: A two-dimensional model, *J. Geophys. Res.*, *91*, 4025–4046, 1986.

Brasseur, G. P., and S. Solomon, *Aeronomy of the Middle Atmosphere*, D. Reidel, Norwell, Mass., 1992.

Brasseur, G. P., A. K. Smith, R. Khosravi, T. Huang, S. Walters, S. Chabrillat, and G. Kockarts, Natural and human-induced perturbations in the middle atmosphere: A short tutorial, in *Atmospheric Science Across the Stratopause*, *Geophys. Monogr. Ser.*, vol. 123, pp. 7–20, edited by D. E. Siskind, S. D. Eckermann, and M. E. Summers, AGU, Washington, D.C., 2000.

Burns, C. J., E. Turunen, H. Matveinen, H. Ranta, and J. K. Hargreaves, Chemical modelling of the quiet summer D- and E-regions using EISCAT electron density profiles, *J. Atmos. Terr. Phys.*, *53*, 115–134, 1991.

Chabrillat, S., Modélisation du changement global dans l'atmosphère moyenne, Ph.D. thesis, Univ. Libre de Bruxelles, Brussells, Belgium, 2001 (available at ftp://ftp.oma.be/dist/simonc/thesis.pdf).

Chabrillat, S., G. Kockarts, D. Fonteyn, and G. P. Brasseur, Impact of molecular diffusion on the CO_2 distribution and the temperature in the mesosphere, *Geophys. Res. Lett.*, *29*(15), 1729, doi:10.1029/2002GL015309, 2002.

Chesnavich, W. J., T. Su, and M. T. Bowers, Collisions in a noncentral field: A variational and trajectory investigation of ion-dipole capture, *J. Chem. Phys.*, *72*, 2641–2655, 1980.

Dotan, I., D. L. Albritton, F. C. Fehsenfeld, G. E. Streit, and E. E. Ferguson, Rate constants for the reactions of O^-, O_2^-, NO_2^-, CO_3^-, and CO_4^- with HCl and ClO^- with NO, NO_2, SO_2 and CO_2 at 300 K, *J. Chem. Phys.*, *68*, 5414–5416, 1978.

Fehsenfeld, F. C., and D. L. Albritton, The role of water vapor in ion chemistry of the atmosphere, in *Atmospheric Water Vapor*, edited by A. Deepak, T. D. Wilkerson, and L. H. Ruhnke, pp. 587–597, Academic, San Diego, Calif., 1980.

Fritzenwallner, J., and E. Kopp, A global D- and E-region ion model, in *Proceedings of the 13th ESA Symposium on European Rocket and Balloon Programmes and Related Research, Öland, Sweden, 26–29 May 1997*, *Eur. Space Agency Spec. Publ.*, *ESA-SP 397*, 375–380, 1997a.

Fritzenwallner, J., and E. Kopp, Chemistry and abundance of main thermospheric metals, in *Proceedings of the 13th ESA Symposium on European Rocket and Balloon Programmes and Related Research, Öland, Sweden, 26–29 May 1997*, *Eur. Space Agency Spec. Publ.*, *ESA-SP 397*, 453–458, 1997b.

Fritzenwallner, J., and E. Kopp, Chlorine and bromine ions in the D-region, *Adv. Space Res.*, *20*, 2111–2115, 1997c.

Fritzenwallner, J., and E. Kopp, Model calculations of the negative ion chemistry in the mesosphere with special emphasis on the chlorine species and the formation of cluster ions, *Adv. Space Res.*, *21*, 891–894, 1998.

Gear, C. W., The automatic integration of stiff ordinary differential equations, in *Information Processing* (*Proceedings of the IFIP Congress 1968*), North-Holland, New York, 1969.

Gear, C. W., *Numerical Initial Value Problems in Ordinary Differential Equations*, Prentice-Hall, Old Tappan, N. J., 1971.

Heaps, M. G., Parametrization of the cosmic ray ion-pair production rate above 18 km, *Planet. Space Sci.*, *26*, 513–517, 1978.

Hedin, A. E., Extension of the MSIS thermospheric model into the middle and lower atmosphere, *J. Geophys. Res.*, *96*, 1159–1172, 1991.

Henke, B. L., E. M. Gullikson, and J. C. Davis, X-ray interactions: Photoabsorption, scattering, transmission, and reflection at E = 50–30,000 eV, Z = 1–92, *At. Data Nucl. Data Tables*, *54*, 181–342, 1993.

Herrmann, U., P. Eberhardt, M. A. Hidalgo, E. Kopp, and L. G. Smith, Metal ions and isotopes in sporadic E-layers during the Perseid meteor shower, in *COSPAR: Space Research*, vol. XVIII, edited by M. L. Mycroft and A. C. Stickland, pp. 249–252, Pergamon, New York, 1978.

Hinteregger, H. E., K. Fukui, and B. R. Gilson, Observational reference and model data on solar EUV, from measurements on AE-E, *Geophys. Res. Lett.*, *8*, 1147–1150, 1981.

Ikezoe, Y., S. Matsuoka, M. Takebe, and A. A. Viggiano, *Gas Phase Ion-Molecule Reaction Rate Constants Through 1986*, Ion Reaction Res. Group, Mass Spectrosc. Soc. of Japan, Tokyo, 1987.

Jacobson, M. Z., *Fundamentals of Atmospheric Modeling*, Cambridge Univ. Press, New York, 1999.

Jones, R. A., and M. H. Rees, Time dependent studies of the aurora - I. Ion density and composition, *Planet. Space Sci.*, *21*, 537–557, 1973.

Jursa, A. S., (Ed.), *Handbook of Geophysics and the Space Environment*, Air Force Geophys. Lab., Hanscom Air Force Base, Mass., 1985.

Kawamoto, H., and T. Ogawa, A steady state model of negative ions in the lower stratosphere, *Planet. Space Sci.*, *32*, 1223–1233, 1984.

Kazil, J., The University of Bern Atmospheric Ion Model: Time-dependent ion modeling in the stratosphere, mesosphere and lower thermosphere, Ph.D. thesis, University of Bern, Bern, Switzerland, 2002.

Keneshea, T. J., R. S. Narcisi, and W. Swider Jr., Diurnal model of the E region, *J. Geophys. Res.*, *75*, 845–854, 1970.

Khosravi, R., G. P. Brasseur, A. K. Smith, D. Rusch, S. Walters, S. Chabrillat, and G. Kockarts, Response of the mesosphere to human perturbations and solar variability calculated by a 2-D model, *J. Geophys. Res.*, *107*(D18), 4358, doi:10.1029/2001JD001235, 2002.

Kopp, E., Positive and negative ions of the middle atmosphere, *Ad. Space Res.*, *12*, (10)325–(10)333, 1992.

Kopp, E., and U. Herrmann, Ion composition in the lower ionosphere, *Ann. Geophys.*, *2*, 83–94, 1984.

Kopp, E., P. Eberhardt, and U. Herrmann, Summer daytime positive ion composition in the D-region above Wallops island, in *COSPAR: Space Research*, vol. XVIII, edited by M. J. Mycroft and A. C. Stickland, pp. 245–248, Pergamon, New York, 1978.

Kopp, E., L. André, and L. G. Smith, Positive ion composition and derived particle heating in the lower auroral ionosphere, *J. Atmos. Terr. Phys.*, *47*, 301–308, 1985.

Kull, A., E. Kopp, G. P. Brasseur, and C. Granier, Ions and electrons in the mesosphere: A model for the quiet D-region, *Adv. Space Res.*, *15*, 2183–2186, 1995.

Kull, A., E. Kopp, G. P. Brasseur, and C. Granier, Ions and electrons of the lower-latitude D region, *J. Geophys. Res.*, *102*, 9705–9716, 1997.

Langevin, P. M., Une formule fondamentale de théorie cinétique, *Ann. Chim. Phys.*, *8*, 245–288, 1905.

Lindzen, R. S., Turbulence and stress owing to gravity wave and tidal breakdown, *J. Geophys. Res.*, *86*, 9707–9714, 1981.

Lübken, F. J., M. J. Jarvis, and G. O. L. Jones, First in situ temperature measurements at the Antarctic summer mesopause, *Geophys. Res. Lett.*, *26*, 3581–3584, 1999.

McCrumb, J. L., and F. Arnold, High-sensitivity detection of negative ions in the stratosphere, *Nature*, *294*, 136–139, 1981.

Mc Ewan, M. J., and L. F. Phillips, *Chemistry of the Atmosphere*, Edward Arnold, London, U.K., 1975.

Mlynczak, M. G., An evaluation of the rate of absorption of solar radiation in the $O_2(X^3\Sigma g \rightarrow b^1\Delta g)$ transition, *Geophys. Res. Lett.*, *20*, 1439–1442, 1993.

Mlynczak, M. G., S. Solomon, and D. S. Zaras, An updated model for $O_2(^1\Delta_g)$ concentrations in the mesosphere and lower thermosphere and implications for remote sensing of ozone at 1.27 μm, *J. Geophys. Res.*, *98*, 18,639–18,648, 1993.

Möhler, O., and F. Arnold, Flow reactor and triple quadrupole mass spectrometer investigations of negative ion reactions involving nitric acid: implications for atmospheric HNO_3 detection by chemical ionization mass spectrometry, *J. Atmos. Chem.*, *13*, 33–61, 1991.

Paulsen, D. E., R. E. Huffman, and J. C. Larrabee, Improved photoionization rates of $O_2(^1\Delta g)$ in the D-region, *Radio Sci.*, *7*, 51–55, 1972.

Preusse, P., S. D. Eckermann, J. Oberheide, M. E. Hagan, and D. Offermann, Modulation of gravity waves by tides as seen in CRISTA temperatures, *Adv. Space Res.*, *27*, 1773–1778, 2001.

Randel, W. J., F. I. Wu, J. M. Russell, A. Roche, and J. W. Waters, Seasonal cycles and QBO variations in stratospheric CH_4 and H_2O observed in UARS HALOE data, *J. Atmos. Sci.*, *55*, 163–185, 1998.

Reid, G. C., Ion chemistry in the D-region, in *Advances in Atomic and Molecular Physics*, vol. 12, edited by D. R. Bates and B. Bederson, pp. 375–413, Academic, San Diego, Calif., 1976.

Reid, G. C., The production of water-cluster positive ions in the quiet daytime D-region, *Planet. Space Sci.*, *25*, 275–290, 1977.

Richards, P. G., J. A. Fennelly, and D. G. Torr, EUVAC: A solar EUV flux model for aeronomic calculations, *J. Geophys. Res.*, *99*, 8981–8992, 1994.

She, C. Y., and U. von Zahn, Concept of a two-level mesopause: Support through new lidar observations, *J. Geophys. Res.*, *103*, 5855–5863, 1998.

Siskind, D. E., and D. W. Rusch, Nitric oxide in the middle to upper atmosphere, *J. Geophys. Res.*, *97*, 3209–3217, 1992.

Siskind, D. E., and J. M. Russell III, Coupling between middle and upper atmospheric NO: Constraints from HALOE observations, *Geophys. Res. Lett.*, *23*, 137–140, 1996.

Siskind, D. E., C. A. Barth, and J. M. Russell III, A climatology of nitric oxide in the mesosphere and lower thermosphere, *Adv. Space Res.*, *21*, 1353–1362, 1998.

Smith, D., N. G. Adams, and E. Alge, Ion-ion mutual neutralization and ion-neutral switching reactions of some stratospheric ions, *Planet. Space Sci.*, *29*, 449–454, 1981.

Smith, L. G., A sequence of rocket observations of night-time sporadic-E, *J. Atmos. Terr. Phys.*, *32*, 1247–1257, 1970.

Solomon, S., P. J. Crutzen, and R. G. Roble, Photochemical coupling between the thermosphere and the lower atmosphere: 1. Odd nitrogen from 50 to 120 km, *J. Geophys. Res.*, *87*, 7206–7220, 1982.

Solomon, S. C., S. M. Bailey, and T. N. Woods, Effect of solar soft X-rays on the lower ionosphere, *Geophys. Res. Lett.*, *28*, 2149–2152, 2001.

Strobel, D. F., T. R. Young, R. R. Meier, T. P. Coffey, and A. W. Ali, The nighttime ionosphere: E region and lower F region, *J. Geophys. Res.*, *79*, 3171–3178, 1974.

Strobel, D. F., C. B. Opal, and R. R. Meier, Photoionization rates in the night-time E- and F-region ionosphere, *Planet. Space Sci.*, *28*, 1027–1033, 1980.

Su, T., Erratum: Trajectory calculations of ion-polar molecule capture rate constants at low temperatures, *J. Chem. Phys.*, *89*, 5355, 1988.

Su, T., and W. J. Chesnavich, Parametrization of the ion-polar molecule collision rate constant by trajectory calculations, *J. Chem. Phys.*, *76*, 5183–5185, 1982.

Thomas, L., NO^+ and water cluster ions in the D-region, *J. Atmos. Terr. Phys.*, *38*, 61–67, 1976a.

Thomas, L., Mesospheric temperatures and and the formation of water cluster ions in the D region, *J. Atmos. Terr. Phys.*, *38*, 1345–1350, 1976b.

Thomas, L., Modeling the ion composition in the middle atmosphere, *Ann. Geophys.*, *1*, 61–73, 1983.

Thomas, L., and M. R. Bowman, Model studies of the D-region negative-ion composition during day-time and night-time, *J. Atmos. Terr. Phys.*, *47*, 547–556, 1985.

Thomas, L., and M. R. Bowman, A study of pre-sunrise changes in negative ions and electrons in the D-region, *Ann. Geophys.*, *4*, 219–228, 1986.

Thomas, L., P. M. Gondhalekar, and M. R. Bowman, The negative-ion composition of the daytime D-region, *J. Atmos. Terr. Phys.*, *35*, 397–404, 1973.

Tobiska, W. K., T. Woods, F. Eparvier, R. Viereck, L. Floyd, D. Bouwer, G. Rottman, and O. R. White, The SOLAR2000 empirical solar irradiance model and forecast tool, *J. Atmos. Sol. Terr. Phys.*, *62*, 1233–1250, 2000.

Tohmatsu, T., and T. Ogawa, *Compendium of Aeronomy*, Terra Sci., Tokyo, 1990.

Torr, M. R., and D. G. Torr, Ionization frequencies for solar cycle 21: Revised, *J. Geophys. Res.*, *90*, 6675–6678, 1985.

Turco, R. P., and C. F. Sechrist Jr., An investigation of the ionospheric D region at sunrise: 1. Time variations of ozone, metastable molecular oxygen, and atomic oxygen, *Radio Sci.*, *7*, 703–716, 1972a.

Turco, R. P., and C. F. Sechrist Jr., An investigation of the ionospheric D region at sunrise: 2. Estimation of some photodetachment rates, *Radio Sci.*, *7*, 717–723, 1972b.

Turco, R. P., and C. F. Sechrist Jr., An investigation of the ionospheric D region at sunrise: 3. Time variations of negative-ion and electron densities, *Radio Sci.*, *7*, 725–737, 1972c.

Turunen, E., High latitude D-region studies by incoherent scatter radar measurements, *Tech. Rep. 52*, Sodankylä Geophys. Obs., 1993.

Turunen, E., H. Matveinen, and H. Ranta, Sodankylä ion chemistry model, *Tech. Rep. 49*, Sodankylä Geophysical Observatory, Sodankylä, Finland, 1993.

Warren, H. P., J. T. Mariska, and K. Wilhelm, High-resolution observations of the solar hydrogen Lyman lines in the quiet sun with the SUMER instrument on SOHO, *Astrophys. J. Suppl. Ser.*, *119*, 105–120, 1998.

Wisemberg, J., and G. Kockarts, Negative ion chemistry in the terrestrial D-region and signal flow graph theory, *J. Geophys. Res.*, *85*, 4642–4652, 1980.

Zbinden, P. A., M. A. Hidalgo, P. Eberhardt, and J. Geiss, Mass spectrometer measurement of the positive ion composition in the D- and E-regions of the ionosphere, *Planet. Space Sci.*, *23*, 1621–1642, 1975.

J. Bishop, Naval Research Laboratory, Code 7643, 4555 Overlook Ave. S.W., Washington, DC 20375, USA. (jbishop@uap2.nrl.navy.mil)

S. Chabrillat, Belgian Institute for Space Aeronomy, Ringlaan-3-Avenue Circulaire, B-1180 Brussels, Belgium. (simonc@oma.be)

J. Kazil, NCAR/HAO, P.O. Box 3000, Boulder, CO 80307-3000, USA. (kazil@ucar.edu)

E. Kopp, Space Research and Planetary Sciences, University of Bern, Sidlerstr. 5, 3012 Bern, Switzerland. (ernest.kopp@space.unibe.ch)